Weak El Niño and Winter Climate in the Mid- to High Latitudes of Eurasia

PENG ZHANG

Department of Atmospheric and Oceanic Sciences & Institute of Atmospheric Sciences, Fudan University, Shanghai, and Earth System Modeling Center, Nanjing University of Information Science and Technology, Nanjing, China

BIN WANG

Earth System Modeling Center, Nanjing University of Information Science and Technology, Nanjing, China, and Department of Atmospheric Sciences and International Pacific Research Center, University of Hawai'i at Mānoa, Honolulu, Hawaii

ZHIWEI WU

Department of Atmospheric and Oceanic Sciences & Institute of Atmospheric Sciences, Fudan University, Shanghai, China

(Manuscript received 28 August 2017, in final form 12 August 2018)

ABSTRACT

According to the sea surface temperature anomaly (SSTA) intensity in the Niño-3.4 region and the east–west gradient across the Pacific, three types of El Niño are identified in this work. An event with larger than average intensity is defined as a strong El Niño, all others are considered to be weak events. Almost all strong El Niños are concurrent with a large gradient, which is featured by negative SSTAs in the western Pacific and positive SSTAs in the equatorial eastern Pacific (EP) and Indian Ocean (IO). According to the east–west gradient, the weak events can be subdivided into gradient-weak (GW) El Niño and equatorial-weak (EW) El Niño. The GW El Niño characterizes a great east–west gradient without a significant IO SSTA. In contrast, the EW event features a positive SSTA over the tropical IO and EP. The impact of GW El Niño on the North Atlantic–Eurasia continent (NA–Eurasia) displays a negative North Atlantic Oscillation (NAO)-like atmospheric anomaly, resulting in a drier and cooler-than-normal winter over Eurasia. Observational and numerical evidence indicate that the prolonged subtropical jet from the North Pacific to NA acts as a waveguide that captures the planetary Rossby waves generated by the GW El Niño. This waveguide favors the propagation of the perturbations into the downstream regions, which would affect the NA–Eurasian climate. However, the EW El Niño is accompanied by a relatively weak subtropical jet that cannot impact the NA–Eurasian climate significantly. For the strong El Niño, the absence of the NAO signal can be attributed to the counteracting of the teleconnections triggered by the Pacific and the tropical IO.

1. Introduction

El Niño–Southern Oscillation (ENSO) is a prominent source of climate predictability that exerts a significant impact on global climate, which has been investigated widely (e.g., Jin et al. 1994; Ropelewski and Halpert 1996; Trenberth and Caron 2000; Wang et al. 2008; Wu et al. 2009; Wu and Li 2009; Wu and Lin 2012). Generally, ENSO can influence the climate over the North Pacific (NP) and North America via the Pacific–North America (PNA) teleconnections (Wallace and Gutzler 1981; Horel and Wallace 1981; Lin and Wu 2011) and can modulate the Asian climate through maintaining the western North Pacific anticyclone anomalies (Wang et al. 2000). However, so far, its impacts on the North Atlantic and Eurasian region (NA–Eurasia) have remained somewhat debatable (Brönnimann 2007; Rodríguez-Fonseca et al. 2016; Polvani et al. 2017).

During the last century, the studies of Ropelewski and Halpert (1987) and Halpert and Ropelewski (1992) suggested that ENSO-related temperature and precipitation anomalies are difficult to detect over the NA–Eurasia region. Several influential factors have been proposed to explain such a nonstationary relationship (Brönnimann 2007), such as the variability of the ENSO signal itself, which may result in different effects in Europe (Greatbatch et al. 2004); tropical volcanic

Corresponding author: Prof. Zhiwei Wu, zhiweiwu@fudan.edu.cn

DOI: 10.1175/JCLI-D-17-0583.1

eruption, which is probably the most important external forcing factor disturbing the ENSO signal (Brönnimann et al. 2007); and some other non-ENSO-related climate factors (Mathieu et al. 2004; Garfinkel and Hartmann 2010). However, such a claim was challenged by subsequent studies (Brönnimann 2007; Ineson and Scaife 2009; Li and Lau 2012). Based on model results, Merkel and Latif (2002) showed that the El Niño events could significantly affect the climate anomalies over Europe—more importantly, the anomalous patterns conform with a negative North Atlantic Oscillation (NAO). This finding has been proven by more recent papers (e.g., Ineson and Scaife 2009; Graf and Zanchettin 2012; Li and Lau 2012), which showed that the wintertime El Niño can excite a negative phase of an NAO-like pattern with colder and drier-than-normal conditions prevailing over Europe (Brönnimann et al. 2007). Some studies further explained that when ENSO events occur, the subtropical jet stream may be activated as a ''bridge'' that connects tropical Pacific and NAO signals (Graf and Zanchettin 2012; Zhang et al. 2015). Other than the roles of the troposphere, the tropical warming excites a polarward-propagating Rossby wave train, which can also extend upward and reach the stratosphere, resulting in a weaker polar vortex that drives a negative NAO anomaly over the NA–Eurasia (e.g., Perlwitz and Graf 1995; Bell et al. 2009; Ineson and Scaife 2009; Butler et al. 2014; Domeisen et al. 2015; Polvani et al. 2017; Richter et al. 2015; Calvo et al. 2017).

Because of the complexity of ENSO itself, the magnitudes and patterns of tropical sea surface temperature anomalies (SSTAs) vary among individual El Niño and La Niña episodes (Capotondi et al. 2015). In particular, the strong ENSO events (especially the so-called ''super El Niños'' such as 1982, 1991, 1997, 2015, etc.) gave rise to extensive damage to property, injuries, and loss of lives. The scientific community thus has paid close attention to these strong events (Schreiber and Schreiber 1984; Philander and Seigel 1985; McPhaden 1999; Wang and Weisberg 2000; L'Heureux et al. 2017; Levine and McPhaden 2016; Paek et al. 2017; and many others). However, what are the possible influences of warm ENSO events with a different intensity? Toniazzo and Scaife (2006) found that the atmospheric anomalies show opposite signs over eastern NA for a strong and moderate El Niño. Recently, Hoell et al. (2016) reported that the precipitation in California is also susceptible to El Niño intensity.

Moreover, according to the locations of anomalous convective centers over the tropical Pacific, the warm ENSO episodes can be defined as the equatorial central Pacific (CP) or the equatorial eastern Pacific (EP) El Niño (Larkin and Harrison 2005; Ashok et al. 2007; Weng et al. 2007; Kao and Yu 2009; Kug et al. 2009). Their opposites are deemed to be the CP or EP La Niña (Cai and Cowan 2009; Shinoda et al. 2011). With different SSTA patterns, the wintertime EP and CP El Niño (La Niña) events exert quite different impacts on the European climate (Graf and Zanchettin 2012; Hurwitz et al. 2014; Zhang et al. 2015). Apart from the shift of the maximum SSTA location, the zonal SST anomalies gradient between the tropical western Pacific (WP) and tropical EP is also an important feature of ENSO (Hoell and Funk 2013). Recently, Wang et al. (2013) proposed a new ENSO-related concept, mega-ENSO, which is defined by using the averaged WP K-shaped SST minus averaged EP triangle SST (Wang et al. 2013, their Fig. 3). Thus, the mega-ENSO not only contains the zonal SST gradient over the tropical WP and tropical EP but also reflects the meridional gradient between the tropical and extratropical Pacific. This new concept has garnered attention from many researchers (Kim and Ha 2015; Wu and Yu 2016; Wu and Zhang 2015; Zhang et al. 2016; Zhang et al. 2017). While considerable efforts have been made to characterize ENSO episodes through tropical Pacific SSTA distribution, few analyses have examined the gradient that exists during ENSO episodes nor have they tried to classify ENSO events depending on the intensity and gradient simultaneously. Here, another question is raised. Does the change of the wintertime ENSO SSTA gradient exert different impacts on the Eurasian climate?

This study aims to investigate the different atmospheric anomalies and their associated climate effects over the NA–Eurasia region during different El Niño events, which are classified by the SSTA intensity in the Niño-3.4 region and the SSTA gradient between the WP and the EP. In this paper, section 2 introduces the data, model, and experiment designs. The ENSO events are first grouped based on the SSTA intensity and second subdivided based on the SST gradient using the Niño-3.4 and mega-ENSO indices in section 3. In section 4, we display the atmospheric responses to different ENSO events over the NA–Eurasia region. Section 5 will discuss the possible mechanisms of how the various categories of El Niño affect the NA–Eurasian climate. The summary and discussion are presented in section 6.

2. Dataset, model, and experiments design

a. Observation data and indices

In this study, the period of datasets used ranges from September 1957 to February 2016, including the

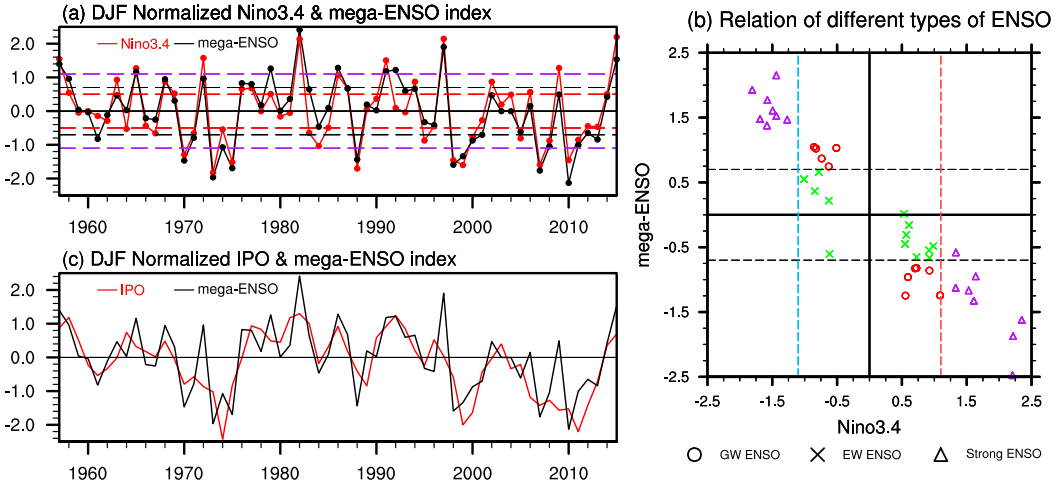

FIG. 1. (a) Time series of the DJF Niño-3.4 and mega-ENSO index. For comparison purposes, the mega-ENSO index is multiplied by −1. (b) Scatter map of the DJF Niño-3.4 and mega-ENSO indices for GW ENSO (red circles), EW ENSO (green crosses), and strong ENSO (purple triangles). The red (blue) dashed line denotes 1.1 (−1.1), and the black dashed line denotes 0.7 (−0.7). (c) Time series of the DJF IPO and mega-ENSO index.

following: 1) monthly SST data from the merged (arithmetic mean) Extended Reconstructed SST, version 4 (ERSST.v4; Huang et al. 2015, 2016; Liu et al. 2015) and the Hadley Centre Sea Ice and Sea Surface Temperature dataset (HadISST; Rayner et al. 2003) with horizontal resolution of 2° × 2°; 2) ERA-40 (Uppala et al. 2005) data for the period of September 1957–February 1979, and ERA-Interim (Dee et al. 2011) from January 1980 to February 2016 with horizontal resolution of 1.5° × 1.5°. The climatological difference between the ERA-40 and ERA-Interim datasets for the period of 1980–2002 is removed from 1980–2016 ERA-Interim data to maintain temporal homogeneity. 3) Monthly global analysis of gauge observations [NOAA Precipitation Reconstruction (PREC); Chen et al. 2002] on a fixed 1.0° × 1.0° longitude–latitude grid; 4) monthly mega-ENSO index (defined within the region of 40°N–40°S, 120°E–90°W) is calculated depending on the definition of Wang et al. (2013); 5) the ENSO events were identified through the Niño-3.4 index (the region of 5°N–5°S, 120°E–170°W), which is defined as the 3-month running mean of merged SSTAs in the Niño-3.4 region based on centered 30-yr base periods (for the method see the website http://www.cpc.noaa.gov/products/analysis_monitoring/ensostuff/ensoyears.shtml); and 6) monthly station-based NAO index (Hurrell 1995). The 1957 winter refers to December 1957 and January–February 1958. The deviation from the average over the ENSO-neutral (normalized Niño-3.4 index between −0.5 and 0.5) years was conducted as the anomalies for all variables. Considering that the surface temperature and precipitation data may contain an upward trend, the data from 1957 to 2015 are detrended to eliminate the long-term trend influence. And the results based on the nondetrended data are nearly the same.

b. *Definition of different types of El Niño events*

The traditional Niño-3.4 index can well represent the intensity of ENSO events but cannot characterize the variation of the ENSO SSTA gradient over the Pacific. The mega-ENSO index is, therefore, introduced to distinguish the El Niño events with a strong or weak gradient. Both indices are shown in Fig. 1a and do not exhibit pronounced trends. The trends of the Niño-3.4 and mega-ENSO indices are −0.007 and 0.0072, respectively—not exceeding the 90% confidence level Mann–Kendall trend significance test (Hamed and Rao 1998; Mondal et al. 2012). On the interannual time scale, the mega-ENSO index is highly correlated with the Niño-3.4 index (the correlation coefficient is 0.9). Compared with the Niño-3.4 index, however, the mega-ENSO index is defined in a very different way. It is calculated by using the averaged west Pacific K-shaped SST minus the averaged east Pacific triangle SST. The Niño-3.4 region is included in the east Pacific triangle region. The mega-ENSO, therefore, is negative for an El Niño. And mega-ENSO shows a spatial pattern similar to the ENSO-like interdecadal variability and the interdecadal Pacific Oscillation (IPO), containing a much broader range than that of conventional ENSO indices.

Figure 1c shows the normalized mega-ENSO and IPO index; their correlation coefficient is −0.74. The IPO index is consistent with the definition given by Dai (2013), which is the second leading EOF of the 3-yr moving-average global SSTs. Although the correlation coefficient of mega-ENSO and IPO is significant, the amplitude in the particular years is quite different. Furthermore, the mega-ENSO contains the SST gradient of the eastern and the western Pacific, which may not be reflected by IPO index. That is why the mega-ENSO index is used in our research.

By the Niño-3.4 and mega-ENSO indices, the steps of grouping El Niño events goes as follows: 1) if a normalized DJF Niño-3.4 index is greater than 0.5, an El Niño winter is considered to occur. The average value of the normalized DJF Niño-3.4 index for these winters is 1.1. Therefore, a year with the normalized DJF Niño-3.4 index greater than 1.1 is defined as a strong El Niño, otherwise, it is considered to be a weak El Niño. The other values between 1 and 1.5 standardized departures of the Niño-3.4 index can also be selected as the threshold, which shows similar results. 2) We group the strong (weak) El Niños depending on the gradient. For the strong gradient El Niño cases, a prerequisite should be satisfied: an El Niño event with a normalized mega-ENSO index less than −0.7. For the weak gradient El Niño, the normalized mega-ENSO index should be more than −0.7. The value of this threshold is chosen after the comparison of the SSTA for each El Niño year (figure not shown). An interesting phenomenon is that almost all strong El Niños have a significant gradient (except 2009, the composite with or without the variables in this year does not influence qualitative results) and only weak El Niños can be subdivided (Fig. 1b). For convenience, the gradient-weak (GW) El Niño and equatorial-weak (EW) El Niño in the text below refer to the weak events with strong and weak gradients. All events are listed in Table 1 as well as the different kinds of La Niña episodes. However, the sample size of GW (EW) La Niñas is too small to obtain a convincing result. That is why, in this manuscript, we mainly pay attention to the warm ENSO events. In Table 1, the CP El Niño years are marked with bold fonts according to the previous studies (e.g., Ashok et al. 2007; Graf and Zanchettin 2012). The CP El Niño seems to be mere random chance among the three types of newly defined El Niño in this study.

We acknowledge that the research samples for three types of El Niño events are quite limited and very likely to be influenced by the large internal variability of the atmosphere, which has a large impact on the ENSO teleconnections (Deser et al. 2017). We perform numerical experiments to investigate the role of SSTAs associated with different types of El Niños in the atmospheric anomalies over the North Atlantic.

TABLE 1. ENSO event classification using the Niño-3.4 and mega-ENSO index. CP El Niño years are set in bold font. El Niño years with sudden stratospheric warmings (SSWs) are set in italic font.

Events		Years
Strong ENSO	El Niño	*1957, **1965**, 1972*, 1982, 1991, 1997, *2009*, 2015 (8)
	La Niña	1970, 1973, 1975, 1988, 1998, 1999, 2007, 2010 (8)
Weak ENSO	GW El Niño	*1958, **1968***, 1976, **1977**, *1979*, ***1986*** (6)
	GW La Niña	1971, 1974, 2000, 2008, 2011 (5)
	EW El Niño	**1963**, *1969, 1987*, **1994**, ***2002***, **2004**, *2006*, 2014 (8)
	EW La Niña	1967, 1983, 1984, 1995, 2005 (5)

c. Simulations

All numerical experiments were performed using an AGCM, the fifth-generation European Centre–Max Plank Institute model (ECHAM5.4; Roeckner et al. 2003). We used the T63L19 version, which features a horizontal resolution of 1.875° and 19 vertical levels. The SST forcing fields were derived from the Atmospheric Model Intercomparison Project (AMIP) II SST and sea ice concentration boundary conditions. In the control run (CTRL), AMIP II historical SST was prescribed for 20 sample years: 1958, 1960, 1961, 1966, 1967, 1969, 1974, 1977, 1979, 1980, 1981, 1985, 1987, 1990, 1996, 2000, 2001, 2003, 2004, and 2006. Almost all of them are weak or neutral ENSO and NAO years (the normalized Niño-3.4 and NAO indices are between −0.7 and 0.7). Therefore, the impact of ENSO and NAO signals could be reduced. The simulations for each sample were integrated for 38 months. Taking 1961 as an example, the simulations were performed for the period from 1 January 1958 to 28 February 1961, the SSTs that matched the 1958–61 time periods. Spinup spans the first 35 months and the last 3-month-average was taken as a sample. To contrast the different climate impacts of the SSTA modes related to the disparate El Niños, we performed a set of sensitivity experiments (see Table 2) with their initial conditions taken from the control experiment. Next, the observational composite SSTA added to the control experiments was prescribed for each sample. At last, 20 ensemble members for each control and sensitivity experiment were considered to reduce the influence of the initial conditions and the internal variability. For the first sensitivity experiment (GW El Niño warming, GW_EN), the composite SST anomaly over the Pacific (40°S–40°N, 120°E–70°W, anomalies are set to zero in the outside region) during

TABLE 2. List of SST perturbation experiments conducted in this study.

Experiments	Description of SST perturbation
GW_EN	SSTA associated with GW El Niño events imposed in the Pacific (40°S–40°N, 120°E–70°W)
EW_EN	SSTA associated with EW El Niño events imposed in the tropical Pacific (20°S–20°N, 160°E–70°W)
EW_EN_IO	SSTA associated with EW El Niño events imposed in the tropical Pacific and Indian Ocean (20°S–20°N, 40°E–70°W)
STRG_EN	SSTA associated with strong El Niño events imposed in the Pacific (40°S–40°N, 120°E–70°W)
IO_WARM	SSTA associated with EW El Niño events imposed in the tropical Indian Ocean (20°S–20°N, 40°–110°E)
STRG_EN_IO	STRG_EN and IO_WARM forcings are imposed together

the GW El Niño winter is added to the control experiments from December to February. To enhance the atmospheric response, we used the SST difference between warm and cold GW ENSO. The prescribed SSTA is similar to the SSTA distributions for GW El Niño (Fig. 2b) but has a larger amplitude. For the second sensitivity experiment (EW El Niño warming, EW_EN), the tropical Pacific SSTA (20°S–20°N, 160°E–70°W) during the EW El Niño winter (EW El Niño minus EW La Niña) is imposed. Since the positive SSTA appears significantly in the Indian Ocean (IO) during the EW El Niño winter, the third experiment (EW_EN_IO) is designed the same way as the EW_EN experiment. However the positive SST anomaly for the EW El Niño is imposed on the IO and Pacific (20°S–20°N, 40°E–70°W) to inspect their combined contribution. For the strong El Niño, another set of experiments is designed. In the fourth experiment (strong El Niño, STRG_EN), we conduct sensitivity simulations where the EP SST warming and WP cooling forcings are both imposed to examine the impact of the strong El Niño. During the strong El Niño, the intensity of the SSTA is much greater than that during the weak El Niño. The SSTA, calculated from strong El Niño minus neutral, is large enough to obtain a clear response in the model. We also study possible contributions of the strong El Niño–related positive SSTA in the tropical IO (20°S–20°N, 40°–110°E) in the fifth experiment (Indian warming,

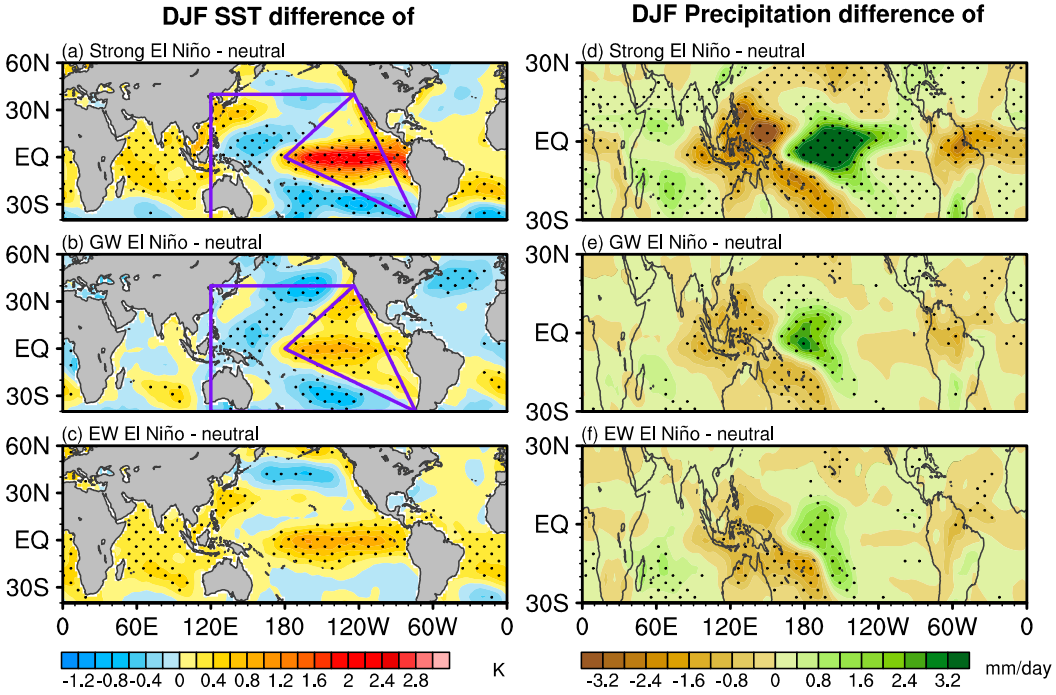

FIG. 2. DJF sea surface temperature (SST; K) composite differences of (a) strong El Niño − neutral, (b) GW El Niño − neutral, and (c) EW El Niño − neutral. Neutral refers to a year in which the Niño-3.4 index is greater than −0.5 and less than 0.5. (d),(e),(f) As in (a), (b) and (c), but for precipitation (mm day^{-1}). The black dots in each panel represent the region with anomalies significant at the 90% confidence level (Student's *t* test). The purple lines in (a) and (b) outline the eastern Pacific triangle and western Pacific K-shaped regions where the mega-ENSO index is defined. Shading intervals are 0.2 K and 0.4 mm day^{-1}.

IO_WARM), as the significant warming SSTAs occur there. In the last experiment (strong El Niño and Indian warming, STRG_EN_IO), we inspected the possible atmospheric response to the combination of IO_WARM and STRG_EN forcings.

3. Comparison of three types of El Niño

The observed large-scale SSTA and tropical precipitation patterns associated with the strong, GW, and EW El Niños are compared in Fig. 2. During a boreal strong El Niño winter, the SSTA shows a "seesaw" mode that highly resembles the mega-ENSO SSTA pattern (purple box in Fig. 2a) with a significant negative anomaly covering the tropical–extratropical WP and a positive SSTA covering the tropical EP. The tropical IO meanwhile shows a significant warming SSTA (Fig. 2a). For the weak El Niño events, two different SSTA patterns are presented: the GW and EW El Niños. In general, the two kinds of weak events have similar SSTA intensity—both are weaker than that during the strong El Niño winter. Specifically, the GW El Niño displays roughly the same pattern in the Pacific as what the strong El Niño shows (purple box in Fig. 2b), but no significant positive SSTA appears in the IO. Conversely, the spatial pattern of the EW El Niño features a highly significant zonal banded warming throughout the tropical oceans from 20°N to 20°S without a significant K-shaped SST cooling in the WP and subtropical Pacific (Fig. 2c).

As expected, the tropical precipitation anomalies related to the three kinds of El Niño are distinct on account of the different SSTA distributions (Figs. 2d–f). For the strong El Niño (Fig. 2d), significant positive rainfall anomalies located mainly over the equatorial CP and EP are accompanied by a relatively dry condition covering the Maritime Continent. This precipitation pattern is in accordance with the result showed by Dai and Wigley (2000, their Fig. 2c). For the weak El Niños, the intensity of tropical Pacific precipitation centers becomes appreciably weaker. During the GW El Niño winter, positive precipitation anomalies straddle the date line with a westward-shifted center and a stronger intensity than that during the EW El Niño winter (Figs. 2e and 2f). Another difference in the precipitation anomaly is that a larger significant negative anomaly appears over the Philippine Sea for the GW El Niño but is not obvious for the EW El Niño. It is interesting to notice that the equatorial CP and EP SSTAs intensity for the GW and EW El Niños (Figs. 2b and 2c) are almost the same. But why does the GW El Niño excite a relatively stronger precipitation anomaly than the EW El Niño?

Rearrangement of convection centers of the Walker circulation during ENSO events induces large precipitation anomalies in the tropics (Dai and Wigley 2000). Thus, to answer the aforementioned question, it is necessary to check the variations of the Walker cell over the equatorial Pacific associated with the GW and EW El Niños. Figure 3 presents the composite maps of the velocity potential and the divergence wind at 850 hPa with respect to the GW and EW El Niños. For the weak events, the vertical movements over the tropical Pacific exhibit an east–west dipole mode. Sinking motion centered over the Maritime Continent and tropical WP features a strong divergence, and the contrary behavior can be detected over the tropical EP. Nevertheless, the convergence over the tropical EP and the divergence over the WP in response to the GW El Niño (Fig. 3a) are stronger than that to the EW El Niño (Fig. 3b). As such, the SSTA for the GW El Niño displays a stronger east–west gradient that can induce a stronger atmospheric response than that for the EW El Niño.

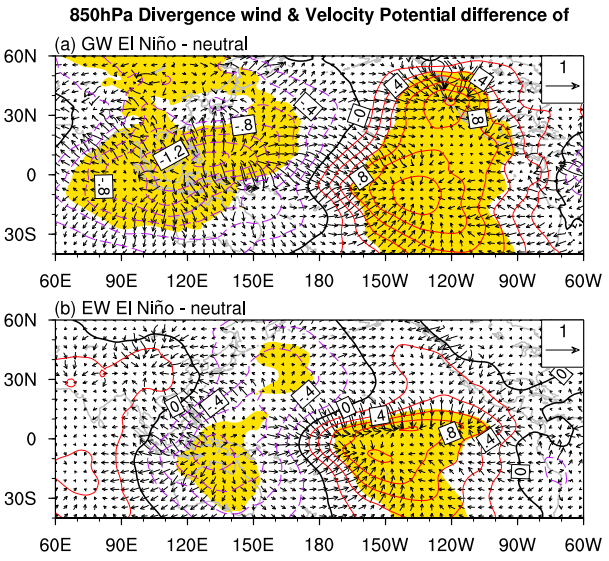

FIG. 3. DJF composite maps of the velocity potential (contour) and the divergence wind (vector) at 850 hPa. (a) GW El Niño − neutral and (b) EW El Niño − neutral. The shadings in each panel represent the region with anomalies significant at the 90% confidence level (Student's *t* test).

4. Atmospheric responses over Eurasia

The different ENSO SST anomaly patterns may give rise to large discrepancies in the extratropical atmospheric circulation as well as regional climate directly by exciting the ENSO teleconnection (Horel and Wallace 1981; Wang et al. 2000; many others) or indirectly through the "atmospheric bridge" (Lau and Nath 1996; Alexander et al. 2002; Graf and Zanchettin 2012). In the present paper, we pay more attention to how the three

kinds of El Niño affect the climate of the Eurasian continent and the mechanism behind them.

Figure 4 compares the large-scale horizontal wind and geopotential height anomalies at 1000 hPa (Z1000, UV1000) for the three kinds of El Niño. As one of the most prominent ENSO teleconnections, the Aleutian low (AL) tends to build up and shifts southeastward during El Niño (Bjerknes 1966, 1969). For the strong events, the AL becomes deeper than that for the weak events, and a PNA-like teleconnection is excited by the strong tropical warming SSTA (Fig. 4a). For the weak El Niños (Figs. 4b,c), compared to the EW El Niño composite, the significant negative Z1000 anomaly over the Aleutian area mildly shifts southeastward during the GW El Niño. However, pronounced discrepancies at Z1000 can be observed over the NA–Eurasia sector. The Z1000 anomaly during the GW El Niño winter shows a negative NAO-like structure (Fig. 5a) with an obvious reinforced anomalous Iceland low and Azores Islands high (Fig. 4b). Nevertheless, the NAO-like pattern disappears during the EW El Niño winter (Fig. 4c). The scatterplot in Fig. 5b displays the relationship between NAO and the three types of El Niño. Five out of six GW warm ENSO episodes occur accompanied by the negative NAO-like patterns, and the exception corresponds to an NAO-neutral pattern (NAO index = −0.05). However, for the strong and EW El Niños, the possibility of the occurrence of a positive or negative NAO-like anomaly is fifty-fifty. This phenomenon indicates that compared to the EW and strong events, the connection of GW El Niño and NAO signals seems more stable.

When an El Niño event occurs concurrently with NAO, their combined effect can lead to even greater or different influences than each of them does alone (Seager et al. 2010; Wu and Lin 2012; Wu and Zhang 2015). Many other works have proven that during winter the NAO signal contributes profoundly to precipitation and surface temperature in NA–Eurasia (Jones et al. 2003; Graf and Zanchettin 2012; Zhang et al. 2015). Figure 6 examines the mean winter (DJF) 2-m air temperature (T2m) and precipitation anomalies of three kinds of El Niño over Eurasia. Great T2m and precipitation differences are found in this region. During the strong El Niño winter, there are no significant T2m anomalies over Eurasia except for central Europe (Fig. 6a). The precipitation anomalies display a monocenter pattern with the significant region mainly located to the northeast of the Caspian Sea (Fig. 6d). During the GW El Niño winter, midlatitude responses show negative T2m anomalies over eastern Europe and northern Asia—up to −2.2 K colder than normal (Fig. 6b). During the EW El Niño winter, no significant T2m anomalies emerge in Eurasia (Fig. 6c). Precipitation-wise, a

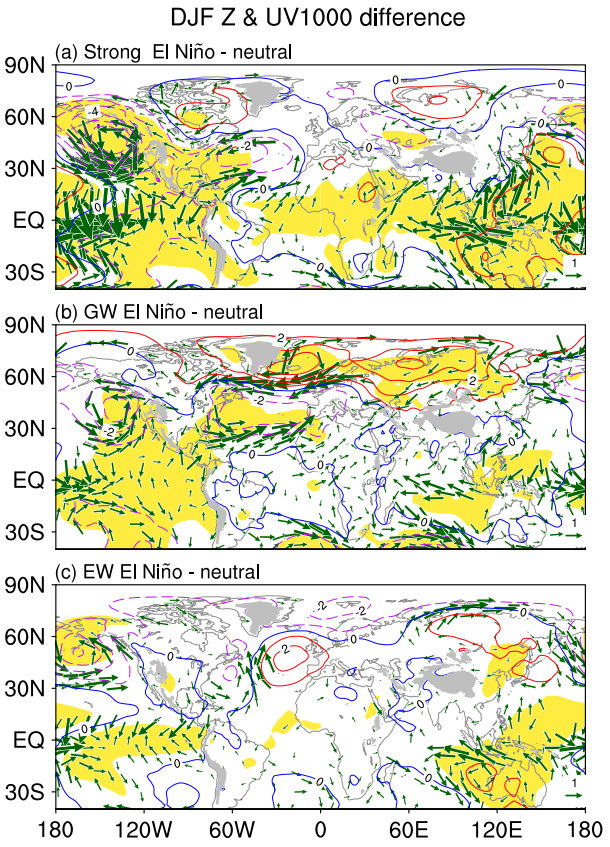

FIG. 4. DJF 1000-hPa geopotential height (Z1000; 10 m) and wind (UV1000; m s^{-1}) composite differences of (a) strong El Niño − neutral, (b) GW El Niño − neutral, and (c) EW El Niño − neutral. The vectors and shadings in each panel represent the region with anomalies significant at the 90% confidence level (Student's *t* test). The contour interval is 10 m.

significant south–north dipole mode is detected during the GW El Niño winter with significant dry conditions controlling northern Eurasia and relatively wet conditions covering southern Eurasia (Fig. 6e). However, for the EW El Niño, there is only a small significant negative anomaly to the south of Lake Baikal (Fig. 6f).

All these phenomena imply that the T2m and precipitation anomalies respond rather differently to the three types of El Niño during the past 59 winters. Among them, the response to GW events is the most significant. Combined with Fig. 4b, the spatial pattern displayed in Figs. 6b and 6e can be explained to some extent. When a GW El Niño event—accompanied by a negative phase of NAO—occurs in the wintertime, the reduced cross-NA westerly flow restricts the warm and moist air blowing from the ocean but favors cold and dry air coming down from the Arctic. This circulation pattern prevails over much of the Eurasian continent, resulting in a colder and drier-than-normal condition

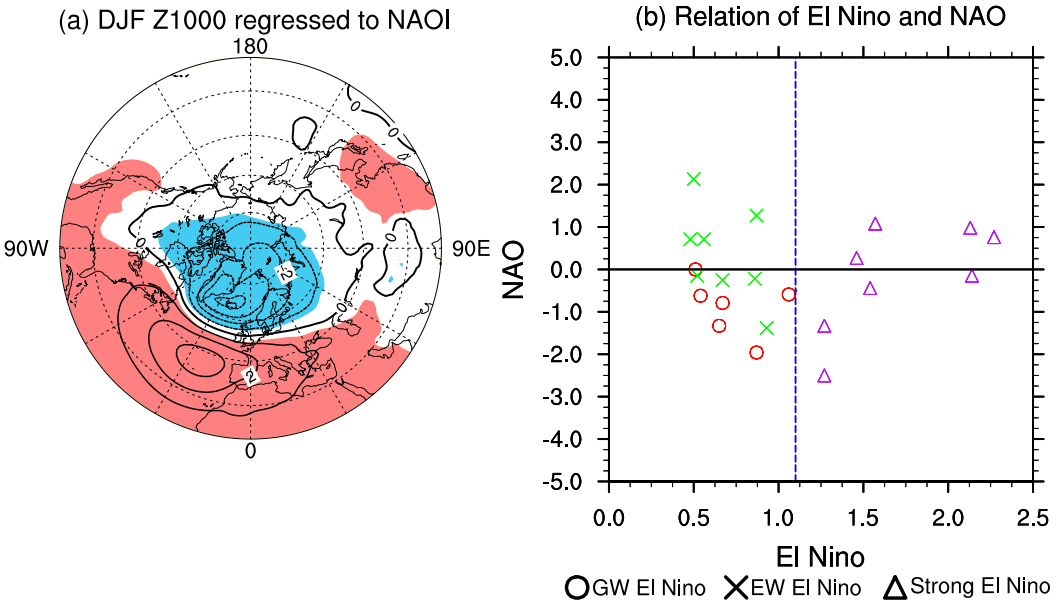

FIG. 5. (a) The regression maps of the Z1000 (10 m) onto the NAO index for 1957–2015. The shadings indicate that the correlations are significant at the 90% confidence levels (Student's *t* test). The contour interval is 10 m. (b) Scatter map of the DJF NAO and Niño-3.4 indices for GW El Niño (red circles), EW El Niño (green crosses), and strong El Niño (purple triangles). The blue dashed line denotes 1.1.

there—in accordance with the demonstration of Hurrell et al. (2003) and Jones et al. (2003). Over southern Eurasia, the positive precipitation anomalies may be induced by the anomalous southerly flow transporting warm and wet air from tropical Africa and the Arabian Sea. And such a pathway through which El Niño impacts the precipitation in southwest central Asia has been discussed by Mariotti (2007). However, during the strong and EW El Niño winters, tropical SSTA cannot exert a significant impact on Eurasia.

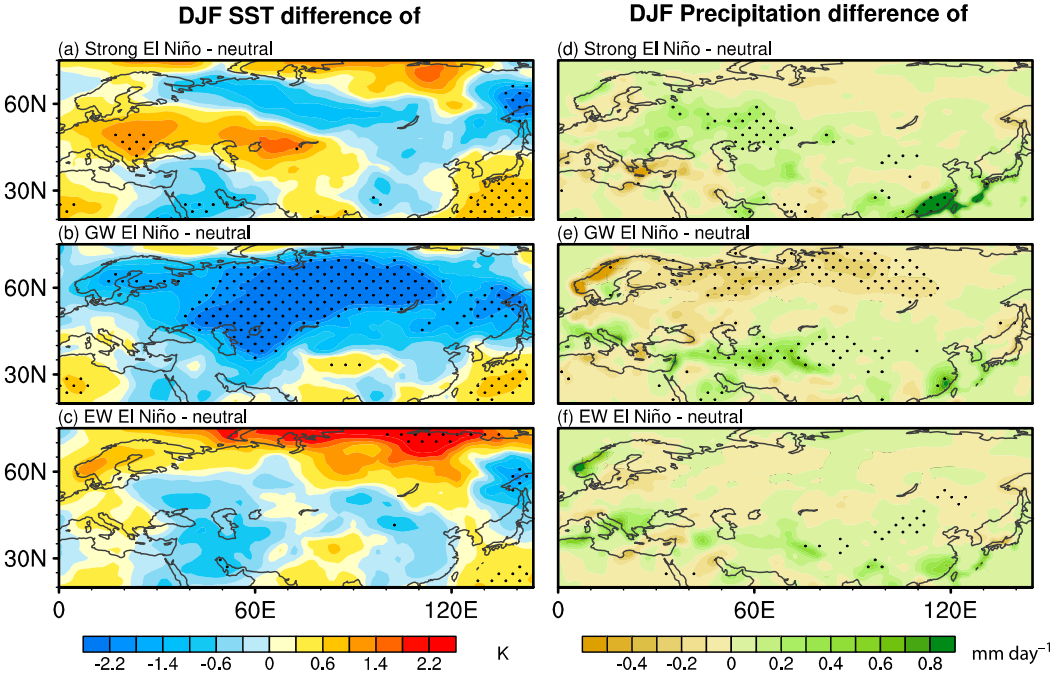

FIG. 6. As in Fig. 2, but for 2-m air temperature (T2m; K) and precipitation (mm day^{-1}) over Eurasia.

For what reasons did the GW El Niño connect with the NAO signal?

It is known that jet streams can affect the propagation of the tropical-induced planetary waves and lead to atmospheric anomalies depending on 1) a strong jet stream acting as a zonal waveguide, 2) the strength of Rossby waves, and 3) the waves that cross the jet streams (Ambrizzi and Hoskins 1997). For an ENSO event, a Rossby wave can be generated by enhanced precipitation and related latent heat released at the equator that propagates from low-latitude regions to the Arctic. When the poleward-propagating Rossby wave crosses the subtropical jet stream, it can be trapped and then the disturbance will propagate downstream along the jet stream waveguide—therefore impacting the downstream region. Graf and Zanchettin (2012) demonstrated that the subtropical jet, as an atmospheric bridge, is of great significance in linking the NAO signal and tropical Pacific warming. Using observational data and numerical simulation, Zhang et al. (2015) verified that the atmospheric bridge also works during the La Niña winter. However, it is still unclear why the GW El Niño connects with the NAO. Whether the subtropical jet can bridge the GW El Niño and NAO teleconnection calls for further investigation. In response, we give the composite 200-hPa zonal wind (U200) anomalies to explore the variations of El Niño–related jet streams (Fig. 7).

From the composite maps, the U200 anomalies—related to the three kinds of El Niño—exhibit a tripolar structure over NP (Fig. 7). In the subtropical NP, significant positive anomalies indicate that the East Asia subtropical jet is strengthened. For the GW El Niño (Fig. 7b), the strengthened anomalous East Asia subtropical jet elongates far eastward from the EP to NA–Eurasia. Significant negative anomalies extend zonally from the extratropical NP to NA, indicating a weakened Atlantic jet. Accompanied by the variations of these two jet streams, a negative NAO-like pattern appears over the NA–Eurasia sector (Fig. 4b). Compared to GW El Niño, the elongations of the two jet streams are not appreciable during the strong El Niño winter. Meanwhile, the cores of two anomalous jet streams over the North American and Atlantic sectors are displaced westward (Fig. 7a). This anomalous U200 pattern resembles that of Graf and Zanchettin (2012, their Fig. 4, middle). For the EW El Niño (Fig. 7c), the upper troposphere subtropical westerly winds become much weaker at the eastern tip of the subtropical jet stream. It suggests that different kinds of El Niño will excite different responses in the East Asian subtropical and Atlantic jets, accompanied by the various atmospheric responses over the NA–Eurasia region (Figs. 4 and 6).

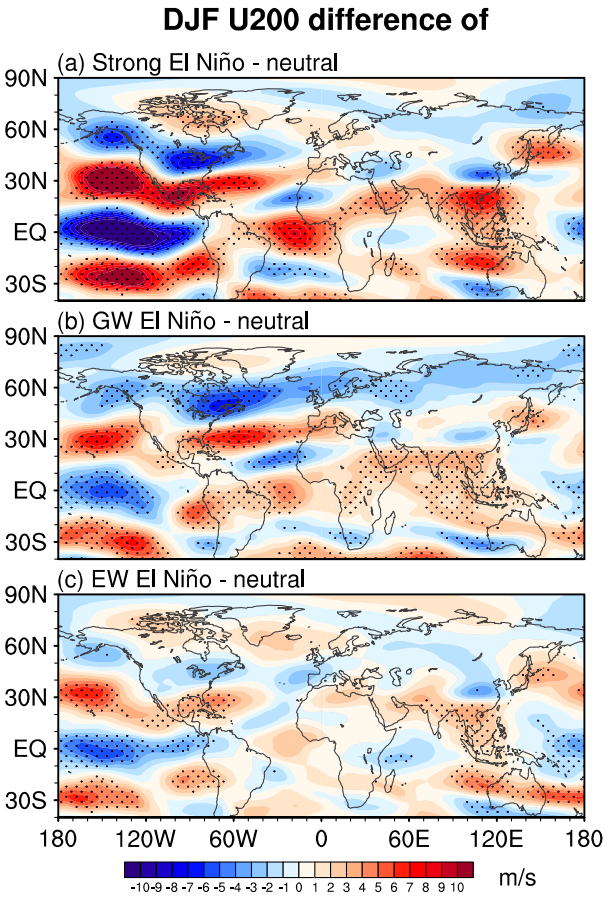

FIG. 7. As in Fig. 2, but for zonal wind ($m\,s^{-1}$) at 200 hPa (U200). The contour interval is $1\,m\,s^{-1}$.

According to the analysis above, we may speculate that El Niño–related jet streams are the key factors to modulating the connection of El Niño and NAO. But the composites do not guarantee any cause and effect. For example, it is hard to tell whether the different responses of the jet streams are caused by the switch of the El Niño types or vice versa. Some researchers have pointed out that the ENSO-related extratropical Pacific SSTAs are excited by the atmosphere, not the opposite way around (Lau and Nath 1990; Alexander et al. 2004). Nevertheless, Robinson (2000) argued that the response of the extratropical atmosphere to underlying SSTAs is weak but not ignorable. Thus, more evidences are needed to confirm causality.

5. Physical mechanisms

Based on the observed analyses above, the different SSTA patterns for the two kinds of weak El Niño are possibly accountable for the two kinds of atmospheric anomalies over NA–Eurasia. To verify the specific

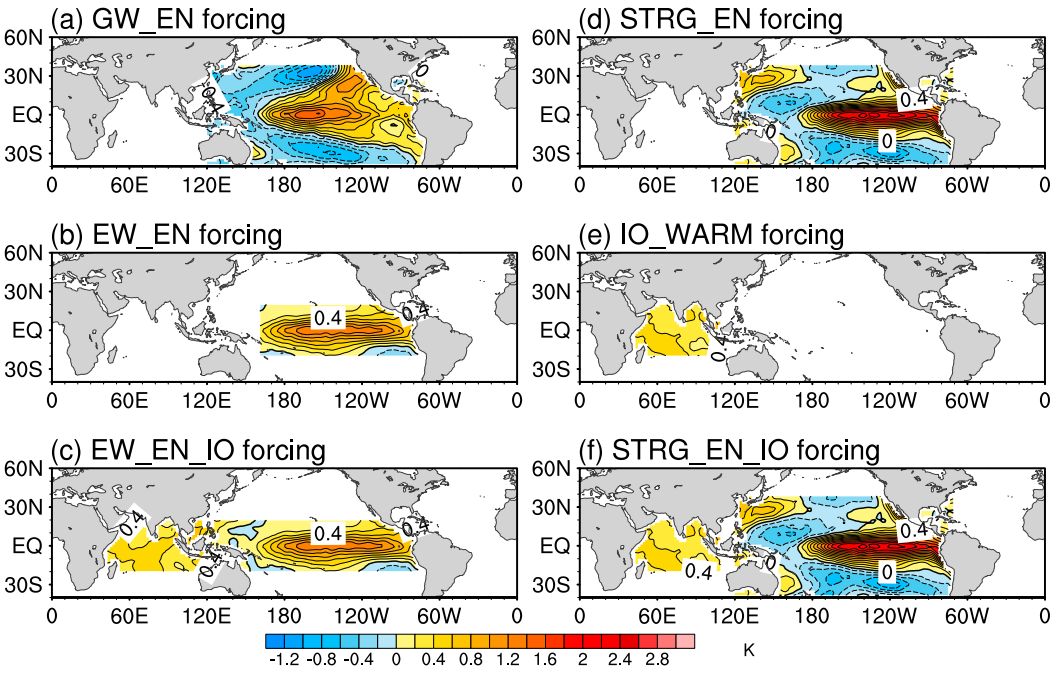

FIG. 8. (a)–(f) The SSTA forcing regions mentioned in Table 2.

processes, a set of experiments was performed—as described in section 2. Figure 8 shows the imposed SSTA for each sensitivity experiment. First, we checked the tropical precipitation response to the GW_EN, EW_EN, and EW_EN_IO forcings relative to the CTRL experiment (Fig. 9). In accordance with the observational results, the imposed EP SST warming, WP and extratropical Pacific cooling in the GW_EN simulation (Fig. 9a) result in stronger tropical Pacific precipitation anomalies than that of the EW_EN and EW_EN_IO simulations (Figs. 9b and 9c). Figure 10 displays the responses of SLP anomalies. The GW_EN SSTA forcing induces a strengthened AL over the NP and a negative NAO-like SLP anomaly over the NA (Fig. 10a). This anomaly pattern markedly resembles the observed GW El Niño composition (Fig. 4b). Under the EW_EN forcing, the anomalous AL is still strong. However, over the NA, the NAO-like atmospheric response disappears (Fig. 10b). Comparing these two simulations, the most obvious difference is that the NAO-like SLP anomaly does not appear in response to the equatorial EP warming without the cooling in the WP K-shaped region. Next, the EW_EN_IO experiment was performed. Considering that an EW El Niño is often observed to occur with an IO SST warming (Fig. 2c), we added a positive IO SSTA to the EW_EN forcing. The result shows a slightly northwestward-shifted AL (Fig. 10c) compared with the GW_EN simulation (Fig. 10a). Meanwhile, the NAO-like atmospheric response is not significant over NA–Eurasia (Fig. 10c)—the outcome basically reproduced the observational result (Fig. 4c). Above all, different SSTA patterns for the two kinds of weak events can result in roughly similar atmospheric responses over the NP. Yet, they trigger quite different responses over the NA.

We speculated above that the GW El Niño is linked to NAO through the subtropical jet stream. Thus, it is necessary to check the jet streams excited by the several kinds of SSTA forcings in the model. The results are shown in Fig. 11. Forced by the GW El Niño SSTA (Fig. 11a), the responses of the jet streams also exhibit a tripolar structure over the NP. Accompanied by a negative NAO-like SLP anomaly over the NA–Eurasia region, a strengthening East Asia subtropical jet and a weakening Atlantic jet extends zonally from the NP to NA–Eurasia. For the EW_EN and EW_EN_IO simulations (Figs. 11b and 11c), the jet streams are unsurprisingly strengthened (weakened) mainly over the NP. Such anomaly patterns are well consistent with the observations (Figs. 7b and 7c). According to the observational and numerical evidence, the mechanism of whether the weak El Niño can link to NAO or not, therefore, can be concluded as follows. During the GW El Niño winter, when the tropical EP warming and the equatorial WP cooling SSTAs are coupled with each other (Fig. 2b), the tropical Pacific precipitation anomalies will be stronger than during the EW El Niño (Figs. 2e and 9a). Also, the anomalous AL in response to

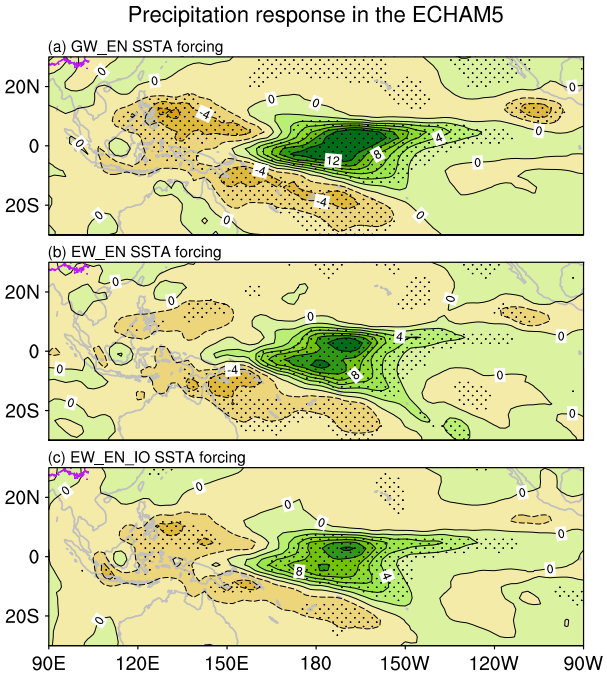

FIG. 9. (a) Tropical precipitation responses in the ECHAM5 regarding a difference between GW_EN forcing and the control run. (b),(c) As in (a), but for EW_EN and EW_EN_IO forcing. The dots in each panel represent the region with anomalies significant at the 90% confidence level (Student's *t* test). The contour interval is 2 mm day^{-1}.

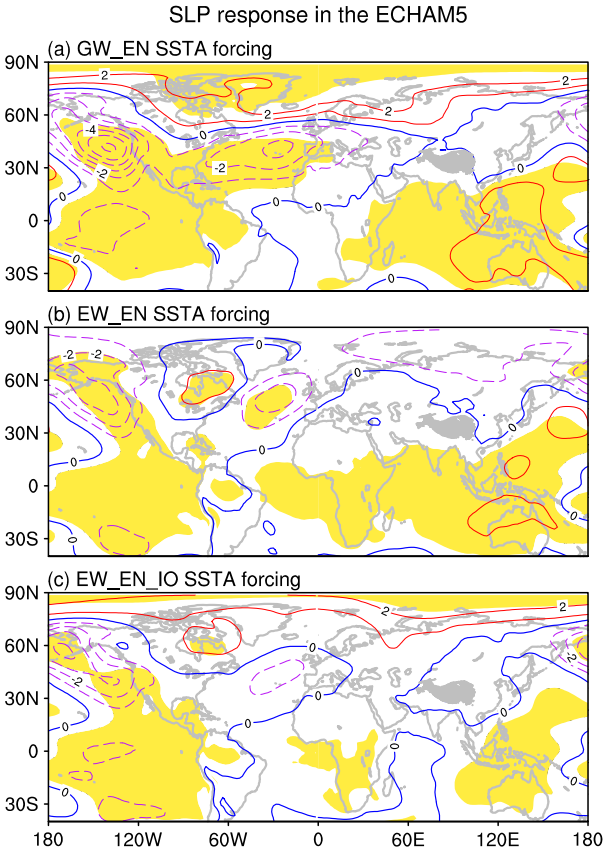

FIG. 10. (a) DJF sea level pressure (SLP) responses in the ECHAM5 regarding a difference between GW_EN forcing and the control run. (b),(c) As in (a), but for EW_EN and EW_EN_IO forcing. The shadings in each panel represent the region with anomalies significant at the 90% confidence level (Student's *t* test). The contour interval is 1 hPa.

the GW El Niño SSTA is located relatively farther east than that of the EW El Niño (Figs. 4b and 10a). Meanwhile, strong abnormal convective heating over tropical oceans excites the subtropical jet elongating zonally from NP to NA–Eurasia. Such circumstances probably enhance the possibility of the planetary Rossby waves, which may be trapped by the subtropical jet stream during their poleward propagation. Along the subtropical jet stream waveguide, some of the perturbation responses will propagate zonally eastward from Pacific sector to the downstream regions and contribute to the weakening of the Azores high and to the negative phase of NAO (Figs. 7b and 11a). The eastward elongated subtropical jet stream cannot be triggered during EW El Niño (Figs. 7c and 11c) when relatively weaker abnormal convective heating occurs near the date line (Figs. 2f and 9c). Under these conditions, the EW El Niño anomaly cannot link with the NAO signal (Figs. 4c and 10c).

Differing from the weak events, the strong El Niño events—especially the so-called super El Niños—have gained wide attention for their significant climate impacts (Wolter and Timlin 1998; Chavez et al. 1999; Lau and Weng 2001; Wu et al. 2010; Christiansen et al. 2016; and so on). From the observations, the strong El Niños are featured by a strong east–west Pacific SSTA gradient and significant IO SST warming (Fig. 2a). We have proven that the GW_EN forcing (with strong east–west SSTA gradient but weaker amplitude in the tropical Pacific than that of STRG_EN forcing) is related to the negative NAO. In previous studies, Hoerling et al. (2004) and Bader and Latif (2005) had proven that imposing a positive SSTA on the tropical IO can induce a positive NAO anomaly. Naturally, we speculate here that the absence of the NAO signal during strong El Niño winter may attribute to the counteracting of the teleconnections excited by the two oceans. Therefore, another set of experiments was performed to examine the possible effects of the different oceans on the NA atmospheric circulation. Figure 12a shows the SLP responses in the STRG_EN simulations relative to the control run. Resembling the GW_EN simulation, the STRG_EN forcing can excite a negative phase of NAO-like SLP anomaly—implying that the linking of El

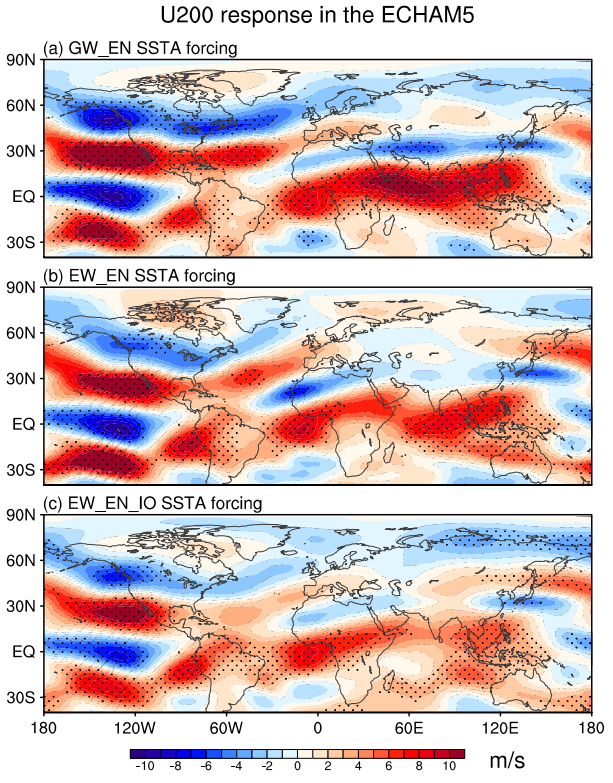

FIG. 11. As in Fig. 10, but for zonal wind at 200 hPa (U200). The dots in each panel represent the region with anomalies significant at the 90% confidence level (Student's t test). The shading interval is 1 m s^{-1}.

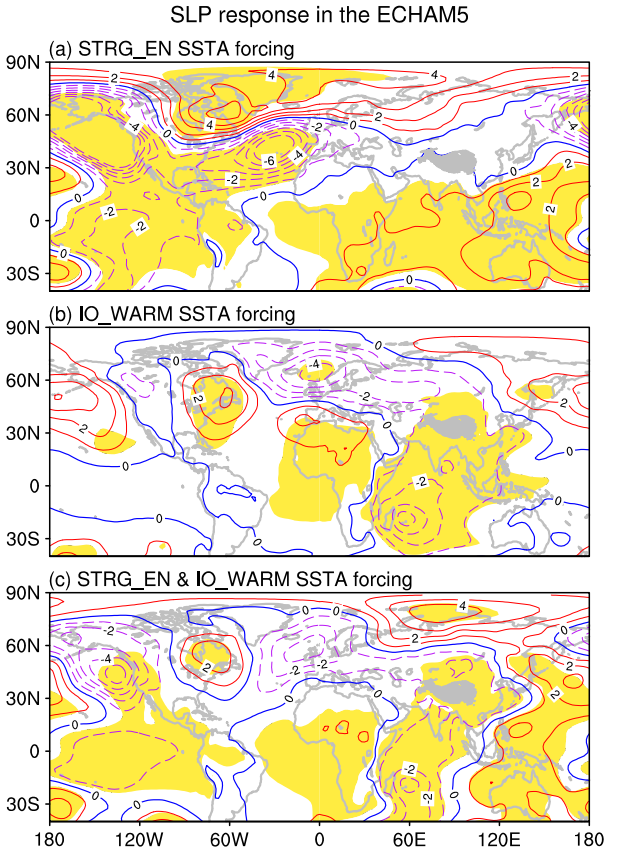

FIG. 12. As in Fig. 10, but for STRG_EN, IO_WARM, and STRG_EN_IO forcing.

Niño and NAO possibly depends on the east–west gradient rather than the amplitude of the tropical Pacific SSTA. Furthermore, we conducted another experiment (IO_WARM), in which the SSTA forcing was only imposed on the tropical IO. In agreement with the previous researches (Hoerling et al. 2004; Bader and Latif 2005), a positive phase of NAO-like response appears over the NA–Eurasia region accompanied by a weakened AL (Fig. 12b). At last, the STRG_EN_IO simulation was conducted, in which the STRG_EN and IO_WARM forcings were both added. The result is displayed in Fig. 12c. Under the STRG_EN_IO forcing, the NAO-like SLP anomaly disappears despite the fact that AL is still strong. The atmospheric responses resemble that of the EW_EN_IO forcing (Fig. 10c). Bader and Latif (2005, hereafter BL05) have revealed that the precipitation response especially near the south equatorial Indian Ocean is characterized by an increase in rainfall due to higher IO SSTs. The mean DJF 300-hPa meridional wind response for the positive IO SSTA forcing resembles the circumglobal pattern, resulting in a positive phase of NAO. Our IO experiment results (not shown) are consistent with what BL05 analyzed. When IO warming induces a positive phase of the NAO and a stronger gradient El Niño induces a negative phase of the NAO, their combined effect might counteract the eastward extension of the subtropical jet over the North Atlantic. It should be noted that in comparison with the observations (Fig. 4a), the SLP responses over North America triggered by the EW_EN_IO forcing are not obvious.

The numerical simulations listed above indicate that the three kinds of warm ENSO episodes exert distinct impacts on the NA–Eurasia atmosphere. The subtropical jet stream serves as an atmospheric bridge and is considered to be one of the key factors in linking the tropical Pacific and the NAO signals during the GW El Niño winter. However, are there any other mechanisms working behind the connection of ENSO and NAO? We have already introduced the stratospheric pathway in linking ENSO and NAO signals in the introduction. The El Niño years with sudden stratospheric warmings (SSWs) are italicized in Table 1 according to the study of Butler et al. (2014) (their Table 1) and Charlton and Polvani (2007). Only half the strong, GW, and EW El Niño years have SSWs. Using ERA reanalysis data, the composite maps of polar cap heights at 50 hPa are also

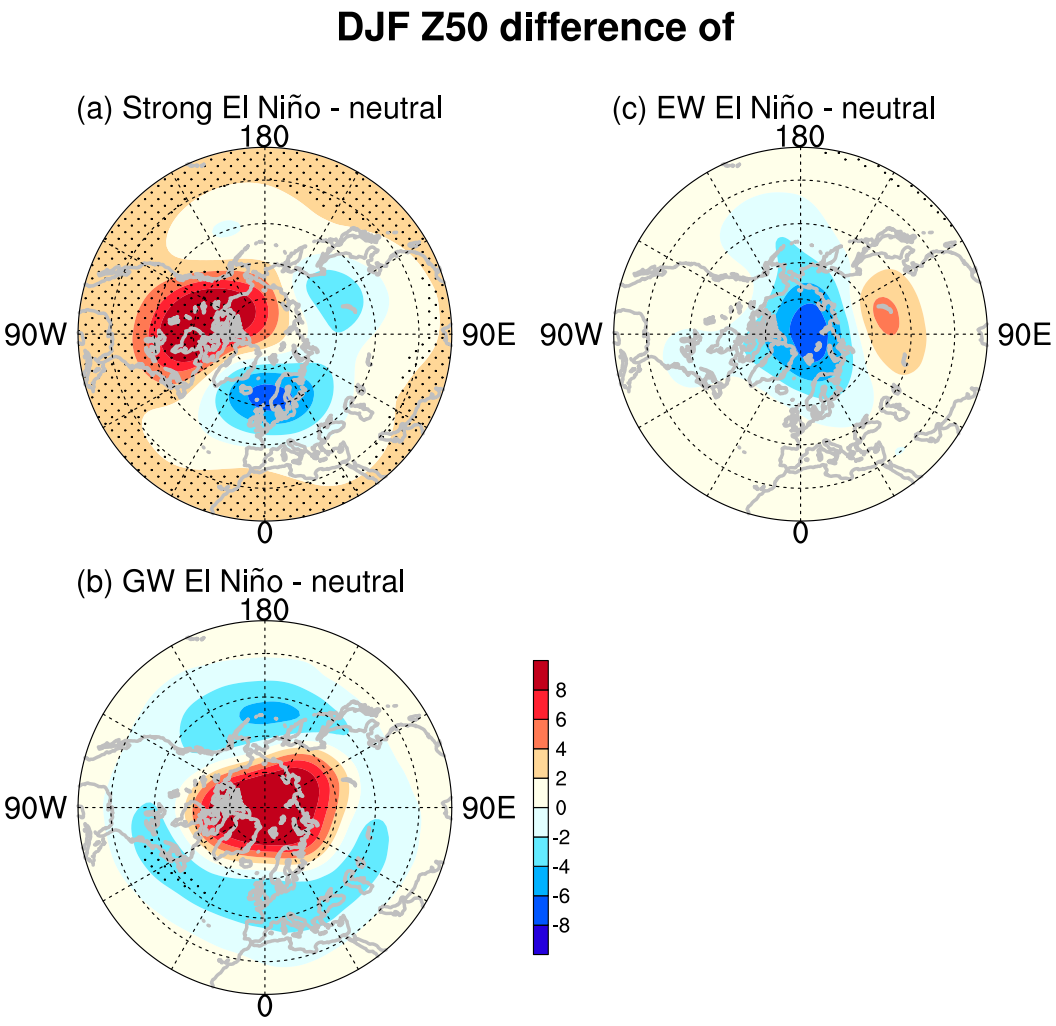

FIG. 13. DJF 50-hPa geopotential height (Z50; 10 m) composite differences of (a) strong El Niño − neutral, (b) GW El Niño − neutral, and (c) EW El Niño − neutral. The dots in each panel represent the region with anomalies significant at the 90% confidence level (Student's *t* test).

displayed to check how the stratosphere is changing in each of El Niño categories (Fig. 13). During strong and EW El Niño winters (Figs. 13a and 13c), neutral or insignificant weak vortices are detected over the polar region. Although the polar vortex became strong for the GW El Niño, the atmospheric anomaly is still insignificant (Fig. 13b). Therefore, compared with the subtropical bridge, stratospheric teleconnection may play a secondary role in the connection of GW El Niño and NAO signals during DJF.

6. Conclusions and discussion

By using Niño-3.4 and mega-ENSO indices, the El Niño events are classified into three types based on the SSTA intensity and gradient (i.e., strong, GW, and EW El Niño). An El Niño with higher-than-average SST intensity in the Niño-3.4 region is defined as a strong event, which features a positive SSTA in the equatorial EP and tropical IO and a negative SSTA in the WP K-shaped region. The strong El Niño events, however, cannot be subdivided depending on the gradient. In contrast, the events with lower-than-average amplitude are defined as a weak El Niño, which is able to be subdivided by the east–west Pacific SSTA gradient. The strong gradient events are referred to as the GW El Niño, which shows an SSTA pattern resembling the strong El Niño without the significant tropical IO SST warming. The weak gradient events are referred to as the EW El Niño, which features a significant zonal banded warming throughout the tropical oceans without a significant negative K-shaped SSTA. These

differences in the amplitude and gradient of SSTA indicate the probability of different fundamental dynamics and climate impacts.

Although the different kinds of weak El Niño can generate a roughly similar atmospheric response over the extratropical NP, markedly different teleconnections are observed over the NA–Eurasia region. During the GW El Niño winter, when EP triangle SST warming is coupled with western K-shaped cooling, a negative NAO-like pattern appears over the NA–Eurasia region accompanied by a weakened Atlantic jet and a strengthened East Asia subtropical jet. This weakened Atlantic jet tends to restrict the moist and warm air from being transported from the Atlantic to the north of Eurasia and induces a much drier and cooler-than-normal winter condition there. However, the NAO-like atmospheric anomaly disappears during the strong and EW El Niño winters along with a neutral Atlantic jet and a relatively weak East Asia subtropical jet. No T2m and precipitation anomalies are detected in Eurasia. Observational and numerical analyses proved that the subtropical jet stream might be a crucial factor in linking the El Niño and NAO signals. The positive mega-ENSO-like SSTA could trigger the East Asia subtropical jet elongating far eastward from NP to NA–Eurasia. This probably enhances the possibility of El Niño–related planetary Rossby waves propagating along the subtropical jet stream waveguides and then affects the downstream regions. During the GW El Niño winter, this is the main pathway to connect ENSO with NAO signals. Moreover, the linkage of ENSO and NAO could also be modulated by the tropical IO. During the strong El Niño winter, the amplitude of SSTA in the Pacific is strong, meanwhile, a positive SSTA is also detected on the tropical IO. For one thing, positive mega-ENSO-like SSTA induces a negative phase of the NAO-like anomaly. For another, previous studies (Hoerling et al. 2004; Bader and Latif 2005) and our numerical results have proved that tropical IO warming may lead to a positive NAO-like atmospheric anomaly. Thus, the combined effect of the Indian and the Pacific Ocean results in an NAO-neutral response over the North Atlantic. For the EW El Niño, the weak subtropical jet stream makes the linkage seem less likely.

To summarize, the different kinds of El Niño would exert different impacts on global climate in the winter time. Through coupling with atmospheric teleconnections, the GW El Niño can exert its influence on the NA–Eurasia regions. But such impacts to the remote areas cannot be detected during the strong and EW El Niño winters. The climatic impacts of the weak El Niño events, therefore, cannot be neglected. Wang et al. (2013) believed that the mega-ENSO is one of the primary sources of the interdecadal variations of the North Hemisphere summer monsoon. Referencing the methods in this study, can the ENSO events in the summertime also be subdivided? Also, what are the mechanisms behind the production of the GW El Niño and EW El Niño? All these questions call for further research.

Acknowledgments. This work is jointly supported by the National Natural Science Foundation of China (NSFC) (Grant 41790475), the National Key Research and Development Program of China (Grant 2016YFA0601801), the Ministry of Science and Technology of China (Grants 2015CB953904 and 2015CB453201), and the NSFC (Grants 91637312, 41575075, 91437216, 61702275, and 41775008). Bin Wang acknowledges support from the National Research Foundation (NRF) of Korea through a Global Research Laboratory (GRL) grant of the Korean Ministry of Education, Science and Technology (MEST, 2011-0021927) and the support from the Atmosphere–Ocean Research Center at the University of Hawaii partially supported by Nanjing University of Information Science and Technology. We thank Dr. Zhiqing Xu and three reviewers for their helpful comments.

REFERENCES

Alexander, M. A., I. Bladé, M. Newman, J. R. Lanzante, N. C. Lau, and J. D. Scott, 2002: The atmospheric bridge: The influence of ENSO teleconnections on air–sea interaction over the global oceans. *J. Climate*, **15**, 2205–2231, https://doi.org/10.1175/1520-0442(2002)015<2205:TABTIO>2.0.CO;2.

——, N. C. Lau, and J. D. Scott, 2004: Broadening the atmospheric bridge paradigm: ENSO teleconnections to the tropical West Pacific–Indian Oceans over the seasonal cycle and to the North Pacific in summer. *Earth's Climate: The Ocean–Atmosphere Interaction*, *Geophys. Monogr.*, Vol. 147, Amer. Geophys. Union, 85–104, https://doi.org/10.1029/147GM05.

Ambrizzi, T., and B. J. Hoskins, 1997: Stationary Rossby-wave propagation in a baroclinic atmosphere. *Quart. J. Roy. Meteor. Soc.*, **123**, 919–928, https://doi.org/10.1002/qj.49712354007.

Ashok, K., S. Behera, A. S. Rao, H. Y. Weng, and T. Yamagata, 2007: El Niño Modoki and its possible teleconnection. *J. Geophys. Res.*, **112**, C11007, https://doi.org/10.1029/2006JC003798.

Bader, J., and M. Latif, 2005: North Atlantic Oscillation response to anomalous Indian Ocean SST in a coupled GCM. *J. Climate*, **18**, 5382–5389, https://doi.org/10.1175/JCLI3577.1.

Bell, C. J., L. J. Gray, A. J. Charlton-Perez, M. M. Joshi, and A. A. Scaife, 2009: Stratospheric communication of El Niño teleconnections to European winter. *J. Climate*, **22**, 4083–4096, https://doi.org/10.1175/2009JCLI2717.1.

Bjerknes, J., 1966: A possible response of the atmospheric Hadley circulation to equatorial anomalies of ocean temperature. *Tellus*, **18**, 820–829, https://doi.org/10.3402/tellusa.v18i4.9712.

——, 1969: Atmospheric teleconnections from the equatorial Pacific. *Mon. Wea. Rev.*, **97**, 163–172, https://doi.org/10.1175/1520-0493(1969)097<0163:ATFTEP>2.3.CO;2.

Brönnimann, S., 2007: Impact of El Niño–Southern Oscillation on European climate. *Rev. Geophys.*, **45**, RG3003, https://doi.org/10.1029/2006RG000199.

——, T. Ewen, T. Griesser, and R. Jenne, 2007: Multidecadal signal of solar variability in the upper troposphere during the 20th century. *Space Sci. Rev.*, **125**, 305–315, https://doi.org/10.1007/s11214-006-9065-2.

Butler, A. H., L. M. Polvani, and C. Deser, 2014: Separating the stratospheric and tropospheric pathways of El Niño–Southern Oscillation teleconnections. *Environ. Res. Lett.*, **9**, 024014, https://doi.org/10.1088/1748-9326/9/2/024014.

Cai, W., and T. Cowan, 2009: La Niña Modoki impacts Australia autumn rainfall variability. *Geophys. Res. Lett.*, **36**, L12805, https://doi.org/10.1029/2009GL037885.

Calvo, N., and Coauthors, 2017: Northern Hemisphere stratospheric pathway of different El Niño flavors in stratosphere-resolving CMIP5 models. *J. Climate*, **30**, 4351–4371, https://doi.org/10.1175/JCLI-D-16-0132.1.

Capotondi, A., and Coauthors, 2015: Understanding ENSO diversity. *Bull. Amer. Meteor. Soc.*, **96**, 921–938, https://doi.org/10.1175/BAMS-D-13-00117.1.

Charlton, A. J., and L. M. Polvani, 2007: A new look at stratospheric sudden warmings. Part I: Climatology and modeling benchmarks. *J. Climate*, **20**, 449–469, https://doi.org/10.1175/JCLI3996.1.

Chavez, F. P., P. G. Strutton, G. E. Friederich, R. A. Feely, G. C. Feldman, D. G. Foley, and M. J. McPhaden, 1999: Biological and chemical response of the equatorial Pacific Ocean to the 1997–98 El Niño. *Science*, **286**, 2126–2131, https://doi.org/10.1126/science.286.5447.2126.

Chen, M., P. Xie, J. Janowiak, and P. A. Arkin, 2002: Global land precipitation: A 50-yr analysis based on gauge observations. *J. Hydrometeor.*, **3**, 249–266, https://doi.org/10.1175/1525-7541(2002)003<0249:GLPAYM>2.0.CO;2.

Christiansen, B., S. Yang, and M. S. Madsen, 2016: Do strong warm ENSO events control the phase of the stratospheric QBO? *Geophys. Res. Lett.*, **43**, 10 489–10 495, https://doi.org/10.1002/2016GL070751.

Dai, A., 2013: The influence of the interdecadal Pacific oscillation on US precipitation during 1923–2010. *Climate Dyn.*, **41**, 633–646, https://doi.org/10.1007/s00382-012-1446-5.

——, and T. M. L. Wigley, 2000: Global patterns of ENSO-induced precipitation. *Geophys. Res. Lett.*, **27**, 1283–1286, https://doi.org/10.1029/1999GL011140.

Dee, D. P., and Coauthors, 2011: The ERA-Interim reanalysis: Configuration and performance of the data assimilation system. *Quart. J. Roy. Meteor. Soc.*, **137**, 553–597, https://doi.org/10.1002/qj.828.

Deser, C., R. Guo, and F. Lehner, 2017: The relative contributions of tropical Pacific sea surface temperatures and atmospheric internal variability to the recent global warming hiatus. *Geophys. Res. Lett.*, **44**, 7945–7954, https://doi.org/10.1002/2017GL074273.

Domeisen, D. I. V., A. H. Butler, K. Fröhlich, M. Bittner, W. A. Müller, and J. Baehr, 2015: Seasonal predictability over Europe arising from El Niño and stratospheric variability in the MPI-ESM seasonal prediction system. *J. Climate*, **28**, 256–271, https://doi.org/10.1175/JCLI-D-14-00207.1.

Garfinkel, C. I., and D. L. Hartmann, 2010: Influence of the quasi-biennial oscillation on the North Pacific and El Niño teleconnections. *J. Geophys. Res.*, **115**, D20116, https://doi.org/10.1029/2010JD014181.

Graf, H.-F., and D. Zanchettin, 2012: Central Pacific El Niño, the "subtropical bridge," and Eurasian climate. *J. Geophys. Res.*, **117**, D01102, https://doi.org/10.1029/2011JD016493.

Greatbatch, R. J., J. Lu, and K. A. Peterson, 2004: Nonstationary impact of ENSO on Euro-Atlantic winter climate. *Geophys. Res. Lett.*, **31**, L02208, https://doi.org/10.1029/2003GL018542.

Halpert, M. S., and C. F. Ropelewski, 1992: Surface temperature patterns associated with the Southern Oscillation. *J. Climate*, **5**, 577–593, https://doi.org/10.1175/1520-0442(1992)005<0577:STPAWT>2.0.CO;2.

Hamed, K. H., and A. R. Rao, 1998: A modified Mann-Kendall trend test for autocorrelated data. *J. Hydrol.*, **204**, 182–196, https://doi.org/10.1016/S0022-1694(97)00125-X.

Hoell, A., and C. Funk, 2013: The ENSO-related west Pacific sea surface temperature gradient. *J. Climate*, **26**, 9545–9562, https://doi.org/10.1175/JCLI-D-12-00344.1.

——, M. Hoerling, J. Eischeid, K. Wolter, R. Dole, J. Perlwitz, T. Xu, and L. Cheng, 2016: Does El Niño intensity matter for California precipitation? *Geophys. Res. Lett.*, **43**, 819–825, https://doi.org/10.1002/2015GL067102.

Hoerling, M. P., J. W. Hurrell, T. Xu, G. T. Bates, and A. Phillips, 2004: Twentieth century North Atlantic climate change. Part II: Understanding the effect of Indian Ocean warming. *Climate Dyn.*, **23**, 391–405, https://doi.org/10.1007/s00382-004-0433-x.

Horel, J. D., and J. M. Wallace, 1981: Planetary-scale atmospheric phenomena associated with the Southern Oscillation. *Mon. Wea. Rev.*, **109**, 813–829, https://doi.org/10.1175/1520-0493(1981)109<0813:PSAPAW>2.0.CO;2.

Huang, B., and Coauthors, 2015: Extended Reconstructed Sea Surface Temperature version 4 (ERSST.v4). Part I: Upgrades and intercomparisons. *J. Climate*, **28**, 911–930, https://doi.org/10.1175/JCLI-D-14-00006.1.

——, and Coauthors, 2016: Further exploring and quantifying uncertainties for Extended Reconstructed Sea Surface Temperature (ERSST) version 4 (v4). *J. Climate*, **29**, 3119–3142, https://doi.org/10.1175/JCLI-D-15-0430.1.

Hurrell, J. W., 1995: Decadal trends in the North Atlantic Oscillation: Regional temperature and precipitation. *Science*, **269**, 676–679, https://doi.org/10.1126/science.269.5224.676.

——, Y. Kushnir, G. Ottersen, and M. Visbeck, 2003: An overview of the North Atlantic oscillation. *The North Atlantic Oscillation: Climatic Significance and Environmental Impact*, *Geophys. Monogr.*, Vol. 134, Amer. Geophys. Union, 1–35, https://doi.org/10.1029/134GM01.

Hurwitz, M. M., N. Calvo, C. I. Garfinkel, A. H. Butler, S. Ineson, C. Cagnazzo, E. Manzini, and C. Peña-Ortiz, 2014: Extra-tropical atmospheric response to ENSO in the CMIP5 models. *Climate Dyn.*, **43**, 3367–3376, https://doi.org/10.1007/s00382-014-2110-z.

Ineson, S., and A. A. Scaife, 2009: The role of the stratosphere in the European climate response to El Niño. *Nat. Geosci.*, **2**, 32–36, https://doi.org/10.1038/ngeo381.

Jin, F. F., J. D. Neelin, and M. Ghil, 1994: El Niño on the devil's staircase: Annual subharmonic steps to chaos. *Science*, **264**, 70–72, https://doi.org/10.1126/science.264.5155.70.

Jones, P. D., T. J. Osborn, and K. R. Briffa, 2003: Pressure-based measures of the North Atlantic Oscillation (NAO): A comparison and an assessment of changes in the strength of the NAO and in its influence on surface climate parameters. *The North Atlantic Oscillation: Climatic Significance and Environmental Impact*, *Geophys. Monogr.*, Vol. 134, 51–62, https://doi.org/10.1029/134GM03.

Kao, H. Y., and J. Y. Yu, 2009: Contrasting eastern-Pacific and central-Pacific types of ENSO. *J. Climate*, **22**, 615–632, https://doi.org/10.1175/2008JCLI2309.1.

Kim, B.-H., and K.-J. Ha, 2015: Observed changes of global and western Pacific precipitation associated with global warming SST mode and mega-ENSO SST mode. *Climate Dyn.*, **45**, 3067–3075, https://doi.org/10.1007/s00382-015-2524-2.

Kug, J. S., F. F. Jin, and S. I. An, 2009: Two types of El Niño events: Cold tongue El Niño and warm pool El Niño. *J. Climate*, **22**, 1499–1515, https://doi.org/10.1175/2008JCLI2624.1.

Larkin, N. K., and D. E. Harrison, 2005: On the definition of El Niño and associated seasonal average U.S. weather anomalies. *Geophys. Res. Lett.*, **32**, L13705, https://doi.org/10.1029/2005GL022738.

Lau, K., and H. Weng, 2001: Coherent modes of global SST and summer rainfall over China: An assessment of the regional impacts of the 1997–98 El Niño. *J. Climate*, **14**, 1294–1308, https://doi.org/10.1175/1520-0442(2001)014<1294:CMOGSA>2.0.CO;2.

Lau, N. C., and M. J. Nath, 1990: A general circulation model study of the atmospheric response to extratropical SST anomalies observed in 1950–79. *J. Climate*, **3**, 965–989, https://doi.org/10.1175/1520-0442(1990)003<0965:AGCMSO>2.0.CO;2.

——, and ——, 1996: The role of the "atmospheric bridge" in linking tropical Pacific ENSO events to extratropical SST anomalies. *J. Climate*, **9**, 2036–2057, https://doi.org/10.1175/1520-0442(1996)009<2036:TROTBI>2.0.CO;2.

Levine, A. F., and M. J. McPhaden, 2016: How the July 2014 easterly wind burst gave the 2015–2016 El Niño a head start. *Geophys. Res. Lett.*, **43**, 6503–6510, https://doi.org/10.1002/2016GL069204.

L'Heureux, M. L., and Coauthors, 2017: Observing and predicting the 2015/16 El Niño. *Bull. Amer. Meteor. Soc.*, **98**, 1363–1382, https://doi.org/10.1175/BAMS-D-16-0009.1.

Li, Y., and N. C. Lau, 2012: Impact of ENSO in the atmospheric variability over the North Atlantic in late winter—Role of transient eddies. *J. Climate*, **25**, 320–342, https://doi.org/10.1175/JCLI-D-11-00037.1.

Lin, H., and Z. Wu, 2011: Contribution of the autumn Tibetan Plateau snow cover to seasonal prediction of North American winter temperature. *J. Climate*, **24**, 2801–2813, https://doi.org/10.1175/2010JCLI3889.1.

Liu, W., and Coauthors, 2015: Extended Reconstructed Sea Surface Temperature version 4 (ERSST.v4). Part II: Parametric and structural uncertainty estimations. *J. Climate*, **28**, 931–951, https://doi.org/10.1175/JCLI-D-14-00007.1.

Mariotti, A., 2007: How ENSO impacts precipitation in southwest central Asia. *Geophys. Res. Lett.*, **34**, L16706, https://doi.org/10.1029/2007GL030078.

Mathieu, P. P., R. T. Sutton, B. W. Dong, and M. Collins, 2004: Predictability of winter climate over the North Atlantic European region during ENSO events. *J. Climate*, **17**, 1953–1974, https://doi.org/10.1175/1520-0442(2004)017<1953:POWCOT>2.0.CO;2.

McPhaden, M. J., 1999: Genesis and evolution of the 1997-98 El Niño. *Science*, **283**, 950–954, https://doi.org/10.1126/science.283.5404.950.

Merkel, U., and M. Latif, 2002: A high resolution AGCM study of the El Niño impact on the North Atlantic/European sector. *Geophys. Res. Lett.*, **29**, 1291, https://doi.org/10.1029/2001GL013726.

Mondal, A., S. Kundu, and A. Mukhopadhyay, 2012: Rainfall trend analysis by Mann-Kendall test: A case study of north-eastern part of Cuttack district, Orissa. *Int. J. Geol. Earth Environ. Sci.*, **2**, 70–78.

Paek, H., J. Y. Yu, and C. Qian, 2017: Why were the 2015/2016 and 1997/1998 extreme El Niños different? *Geophys. Res. Lett.*, **44**, 1848–1856, https://doi.org/10.1002/2016GL071515.

Perlwitz, J., and H. F. Graf, 1995: The statistical connection between tropospheric and stratospheric circulation of the Northern Hemisphere in winter. *J. Climate*, **8**, 2281–2295, https://doi.org/10.1175/1520-0442(1995)008<2281:TSCBTA>2.0.CO;2.

Philander, S. G., and A. D. Seigel, 1985: Simulation of El Niño of 1982–1983. *Coupled Ocean–Atmosphere Models*, J. C. J. Nihoul, Ed., Elsevier Oceanography Series, Vol. 40, Elsevier, 517–541, https://doi.org/10.1016/S0422-9894(08)70729-3.

Polvani, L. M., L. Sun, A. H. Butler, J. H. Richter, and C. Deser, 2017: Distinguishing stratospheric sudden warmings from ENSO as key drivers of wintertime climate variability over the North Atlantic and Eurasia. *J. Climate*, **30**, 1959–1969, https://doi.org/10.1175/JCLI-D-16-0277.1.

Rayner, N. A., D. E. Parker, E. B. Horton, C. K. Folland, L. V. Alexander, D. P. Rowell, E. C. Kent, and A. Kaplan, 2003: Global analyses of sea surface temperature, sea ice, and night marine air temperatures since the late nineteenth century. *J. Geophys. Res.*, **108**, 4407, https://doi.org/10.1029/2002JD002670.

Richter, J. H., C. Deser, and L. Sun, 2015: Effects of stratospheric variability on El Niño teleconnections. *Environ. Res. Lett.*, **10**, 124021, https://doi.org/10.1088/1748-9326/10/12/124021.

Robinson, W. A., 2000: Review of EWTS—The workshop on extratropical SST anomalies. *Bull. Amer. Meteor. Soc.*, **81**, 567–577, https://doi.org/10.1175/1520-0477(2000)081<0567:ROWTWO>2.3.CO;2.

Rodríguez-Fonseca, B., and Coauthors, 2016: A review of ENSO influence on the North Atlantic. A non-stationary signal. *Atmosphere*, **7**, 87–105, https://doi.org/10.3390/atmos7070087.

Roeckner, E., and Coauthors, 2003: The atmospheric general circulation model ECHAM5. Part I: Model description. Max Planck Institute Rep. 349, 140 pp.

Ropelewski, C. F., and M. S. Halpert, 1987: Global and regional scale precipitation patterns associated with the El Niño/Southern Oscillation. *Mon. Wea. Rev.*, **115**, 1606–1626, https://doi.org/10.1175/1520-0493(1987)115<1606:GARSPP>2.0.CO;2.

——, and ——, 1996: Quantifying Southern Oscillation–precipitation relationships. *J. Climate*, **9**, 1043–1059, https://doi.org/10.1175/1520-0442(1996)009<1043:QSOPR>2.0.CO;2.

Schreiber, R. W., and E. A. Schreiber, 1984: Central Pacific seabirds and the El Niño southern oscillation: 1982 to 1983 perspectives. *Science*, **225**, 713–716, https://doi.org/10.1126/science.225.4663.713.

Seager, R., Y. Kushnir, J. Nakamura, M. Ting, and N. Naik, 2010: Northern Hemisphere winter snow anomalies: ENSO, NAO and the winter of 2009/10. *Geophys. Res. Lett.*, **37**, L14703, https://doi.org/10.1029/2010GL043830.

Shinoda, T., H. E. Hurlburt, and E. J. Metzger, 2011: Anomalous tropical ocean circulation associated with La Niña Modoki. *J. Geophys. Res.*, **116**, C12001, https://doi.org/10.1029/2011JC007304.

Toniazzo, T., and A. A. Scaife, 2006: The influence of ENSO on winter North Atlantic climate. *Geophys. Res. Lett.*, **33**, L24704, https://doi.org/10.1029/2006GL027881.

Trenberth, K. E., and J. M. Caron, 2000: The Southern Oscillation revisited: Sea level pressure, surface temperatures, and precipitation. *J. Climate*, **13**, 4358–4365, https://doi.org/10.1175/1520-0442(2000)013<4358:TSORSL>2.0.CO;2.

Uppala, S. M., and Coauthors, 2005: The ERA-40 re-analysis. *Quart. J. Roy. Meteor. Soc.*, **131**, 2961–3012, https://doi.org/10.1256/qj.04.176.

Wallace, J. M., and D. S. Gutzler, 1981: Teleconnections in the geopotential height field during the Northern Hemisphere winter. *Mon. Wea. Rev.*, **109**, 784–812, https://doi.org/10.1175/1520-0493(1981)109<0784:TITGHF>2.0.CO;2.

Wang, B., R. G. Wu, and X. H. Fu, 2000: Pacific–East Asia teleconnection: How does ENSO affect East Asian climate? *J. Climate*, **13**, 1517–1536, https://doi.org/10.1175/1520-0442(2000)013<1517:PEATHD>2.0.CO;2.

——, Z. Wu, J. Li, J. Liu, C. P. Chang, Y. H. Ding, and G. X. Wu, 2008: How to measure the strength of the East Asian summer monsoon? *J. Climate*, **21**, 4449–4463, https://doi.org/10.1175/2008JCLI2183.1.

——, J. Liu, H. J. Kim, P. J. Webster, S. Y. Yim, and B. Q. Xiang, 2013: Northern Hemisphere summer monsoon intensified by mega-El Niño/southern oscillation and Atlantic multidecadal oscillation. *Proc. Natl. Acad. Sci. USA*, **110**, 5347–5352, https://doi.org/10.1073/pnas.1219405110.

Wang, C., and R. H. Weisberg, 2000: The 1997–98 El Niño evolution relative to previous El Niño events. *J. Climate*, **13**, 488–501, https://doi.org/10.1175/1520-0442(2000)013<0488:TENOER>2.0.CO;2.

Weng, H., K. Ashok, S. K. Behera, A. S. Rao, and T. Yamagata, 2007: Impacts of recent El Niño Modoki on dry/wet conditions in the Pacific rim during boreal summer. *Climate Dyn.*, **29**, 113–129, https://doi.org/10.1007/s00382-007-0234-0.

Wolter, K., and M. S. Timlin, 1998: Measuring the strength of ENSO events: How does 1997/98 rank? *Weather*, **53**, 315–324, https://doi.org/10.1002/j.1477-8696.1998.tb06408.x.

Wu, B., T. Li, and T. J. Zhou, 2010: Relative contributions of the Indian Ocean and local SST anomalies to the maintenance of the western North Pacific anomalous anticyclone during the El Niño decaying summer. *J. Climate*, **23**, 2974–2986, https://doi.org/10.1175/2010JCLI3300.1.

Wu, Z., and J. Li, 2009: Seasonal prediction of the global precipitation annual modes with the grid-point atmospheric model of IAP LASG (GAMIL). *Acta Meteor. Sin.*, **23**, 428–437.

——, and H. Lin, 2012: Interdecadal variability of the ENSO-North Atlantic Oscillation connection in boreal summer. *Quart. J. Roy. Meteor. Soc.*, **138**, 1668–1675, https://doi.org/10.1002/qj.1889.

——, and P. Zhang, 2015: Interdecadal variability of the mega-ENSO–NAO synchronization in winter. *Climate Dyn.*, **45**, 1117–1128, https://doi.org/10.1007/s00382-014-2361-8.

——, and L. Yu, 2016: Seasonal prediction of the East Asian summer monsoon with a partial-least square model. *Climate Dyn.*, **46**, 3067–3078, https://doi.org/10.1007/s00382-015-2753-4.

——, B. Wang, J. Li, and F. F. Jin, 2009: An emperical seasonal prediction model of the East Asian summer monsoon using ENSO and NAO. *J. Geophys. Res.*, **114**, D18120, https://doi.org/10.1029/2009JD011733.

Zhang, L., Z. Wu, and Y. Zhou, 2016: Different impacts of typical and atypical ENSO on the Indian summer rainfall: ENSO-developing phase. *Atmos.–Ocean*, **54**, 440–456, https://doi.org/10.1080/07055900.2016.1209156.

Zhang, P., Z. Wu, and H. Chen, 2017: Interdecadal variability of the ENSO–North Pacific atmospheric circulation in winter. *Atmos.–Ocean*, **55**, 110–120, https://doi.org/10.1080/07055900.2017.1291411.

Zhang, W. J., L. Wang, B. Q. Xiang, L. Qi, and J. H. He, 2015: Impacts of two types of La Niña on the NAO during boreal winter. *Climate Dyn.*, **44**, 1351–1366, https://doi.org/10.1007/s00382-014-2155-z.